Chapter 4
Electrooxidation of Ethanol on Nickel-Copper Multilayer Metal Hydroxide Electrode

Antonina A. Maizelis

4.1 Introduction

The electrocatalytic oxidation of some alcohols is of great interest due to a wide range of application. The reaction is used not only in electrosynthesis of organic compounds but in direct alcohol fuel cells (DAFCs) too. Fuel cells require highly reactive fuels with high-energy density and low toxicity [1–4]. One of the key points to develop a cost-effective electrolysis is to decrease the cost of electrocatalysts for the oxidation. The commercial use of highly effective catalysts containing Pt and Pd is limited due to having high cost and global scarcity [5]. Alkaline electrolytes allow the use of inexpensive transitional metals and metal oxides. Such electrolytes have higher efficiency of both anodic and cathodic processes. There is almost no sensitivity to the surface structure and negligible poisoning effects in alkaline solutions [4].

Among the most promising alternative catalytic materials are cheap Ni-based catalysts having excellent electrochemical activity, stability, and high catalytic abilities toward the alcohol oxidation reaction [6–12]. The electrochemical behavior of electrode made of pure copper and other different copper-based composite electrodes has been studied toward alcohol oxidation in alkaline medium [2, 13, 14]. The copper-nickel alloy is proposed as potential substrate for production of anode component of fuel cells [15]. The methanol electrooxidation at the Ni-Cu alloy (40% Cu)-modified electrode was significantly larger than that at pure Ni [16–18].

To increase the surface area of electrode, the highly porous metallic nickel matrices as Raney electrodes, carbon-supporting materials such as graphene, carbon nanofibers (CNFs), mesoporous carbon, carbon nanotubes (CNTs), and

A. A. Maizelis (✉)
National Technical University "Kharkiv Polytechnic Institute", Kharkiv, Ukraine

O. Fesenko, L. Yatsenko (eds.), *Nanocomposites, Nanostructures, and Their Applications*, Springer Proceedings in Physics 221,
https://doi.org/10.1007/978-3-030-17759-1_4

noncarbonaceous-based materials such as hybrid supports materials and conducting polymers are proposed [5, 19, 20].

In this chapter the results of the study of catalytic activity of the multilayer nickel-copper metal hydroxide electrode with an electrochemically accessible developed surface is presented. Electrode coating was electrodeposited in polyligand pyrophosphate-ammonia electrolyte that allows to obtain multilayer nickel-copper coating with high adhesion to various substrates [21, 22], good mechanical properties [23, 24], and catalytic activity in the oxidation of methanol [25].

4.2 Experimental

Multilayer coatings were deposited in pyrophosphate-ammonia polyligand electrolyte containing 0.1 mol L^{-1} $CuSO_4 \cdot 5H_2O$, 0.5 mol L^{-1} $NiSO_4 \cdot 7H_2O$, 1.0 mol L^{-1} $K_4P_2O_7$, 4.0 mol L^{-1} ammonia as a mixture of 0.4 mol L^{-1} NH_4Cl, and 3.6 mol L^{-1} NH_4OH, pH 8.5. The counter electrode was combined of copper and nickel. The obtained multilayer coatings were tested in electrolyte containing 1 mol L^{-1} KOH and electrolyte additionally containing 0.5 mol L^{-1} ethanol. Electrochemical studies were carried out using potentiostat P-45X. The working electrodes were made of copper wire with an open surface area of 0.152 cm^2. The real surface area of the electrodes with and without coating in the stabilized oxidized state was determined by electrochemical double layer capacitance measurements using cyclic voltammetry (CVA) in 0.5 KOH by the method used in [26] taking in account for comparison the capacity of the oxidized metal surface as 60 mkF cm^{-2}. The counter electrode was made of platinum. A saturated silver/silver chloride electrode was used as the reference electrode.

4.3 Experimenal Results and Discussion

On the CVA curve (Fig. 4.1) on a platinum electrode (staring potentials scan in the cathode direction), there is a wave of limiting current of copper deposition (in the potential range of $-0.45 \ldots -0.85$ V). Then (in the potential range of $-1.19 \ldots -1.25$ V) a wave of limiting current of a nickel-copper alloy deposition appears. After it (under conditions of intensive hydrogen evolution), the copper and nickel hydroxy compounds as well as hydrides deposit with alloy. When scanning potentials in the anodic direction, the alloy deposition is facilitated due to both surface development and its enrichment with nickel. At the first peak of the anode branch of the CVA, the copper-rich phase dissolves from the deposit. Then nickel-rich phase dissolves in the second peak. The copper content in the coating (33%) was determined similarly to [27, 28] by the method of anodic voltammetry in an ammonia-glycinate electrolyte, which allows selective dissolution of copper and nickel.

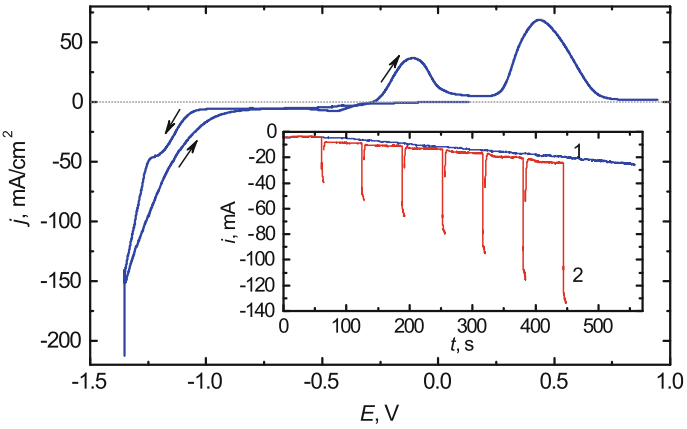

Fig. 4.1 CVA on Pt in pyrophosphate-ammonia electrolyte. Potential scan rate is $10\,\mathrm{mV\,s^{-1}}$. Insert: $E-t$ curves of Ni-Cu alloy coating deposition (1) at a potential of -1.175 V and NiCu(ML) coating deposition (2)

The multilayer nickel-copper metal hydroxide coating NiCu(ML) was formed by a two-pulse potentiostatic method with periodic potential change from -1.175 V (between two limiting currents on CVA Fig. 4.1) to -1.35 V (above the second wave). In this case the nickel-copper alloy layer is deposited at potential of -1.175 V, and the layer containing mixture of metals and its hydroxides is deposited at potential of -1.35 VV. Insert at Fig. 4.1 shows the chronoamperograms of multilayer coating deposition (curve 1) and nickel-copper alloy coating deposition at potential of -1.175 V (curve 1). The deposition current increases in both cases, indicating the increase in surface area of the samples during the deposition process both at potential of -1.35 V and at a potential of -1.175 V. Both coatings were deposited until the deposition current at potential of -1.175 V reached 24 mA. Therefore the samples with coating had approximately the same surface area available for deposition. The approximate calculated thickness of alloy layers varies from 430 to 110 nm. The thickness of metal hydroxide layers decreases from 260 to 40 nm during electrodeposition. For comparison, a sample with porous nickel coating electrodeposited in Watts bath was obtained.

After coating deposition all the samples were cycled in 1 M KOH solution (Fig. 4.2) in the range potentials corresponding to the reaction [6]:

$$Ni(OH)_2 \rightarrow NiOOH + H^+ + e^-. \tag{4.1}$$

The oxidation current in the first cycle at the initial section of anodic branch of CVA is much higher on the samples with alloy coating (curve 2) and multilayer coating (curve 1) than on nickel surface (curve 3) due to more active oxidation of copper in this region of potentials. The anodic peak of the first cycle is located at more positive potentials than the peaks of subsequent cycles on all samples. The

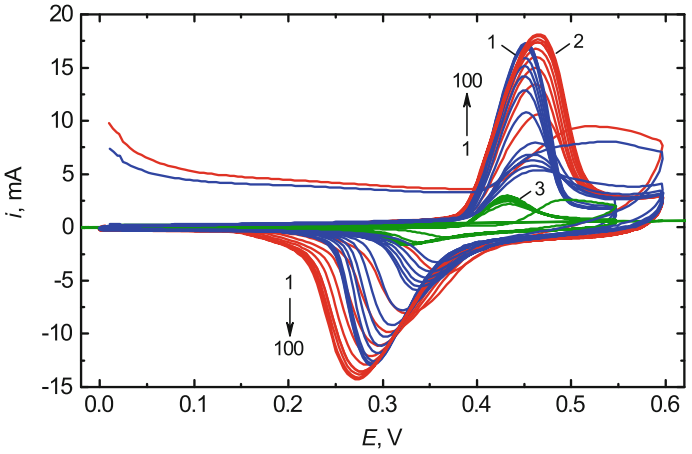

Fig. 4.2 CVA in 1 mol L^{-1} KOH on electrodes with NiCu(ML) (1), Ni-Cu alloy (2), and Ni (3) coatings. Potential scanning rate of 50 mV s^{-1}. Every 10th cycle is shown

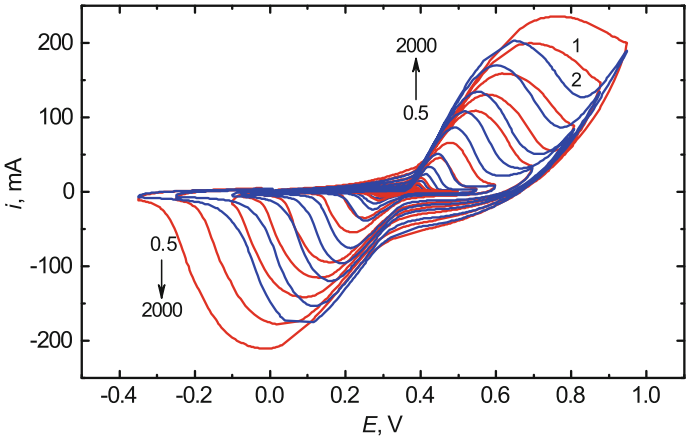

Fig. 4.3 CVA in 1 mol L^{-1} KOH on electrodes with NiCu(ML) (1) and Ni-Cu alloy (2) coatings

height of the anodic and cathodic peaks corresponding to the flow of reaction (1) in the cathodic and anodic directions increases. As the surface of the samples is saturated with active sites, the height of these peaks stabilizes. Further studies were performed on the stabilized surface of the electrodes. The real area of the stabilized surface of the electrodes, determined out of capacity value, was 5.0 and 5.26 cm^2 for samples with Ni-Cu alloy and NiCu (ML) coatings, respectively.

As the potential scan rate increases from 0.5 to 2000 mV s^{-1} (Figs. 4.3 and 4.4), the height of both the cathode and anode peaks increases. The potential difference between them also increases, indicating increase in the degree of irreversibility of redox processes on all investigated electrodes. The height of the peaks linearly

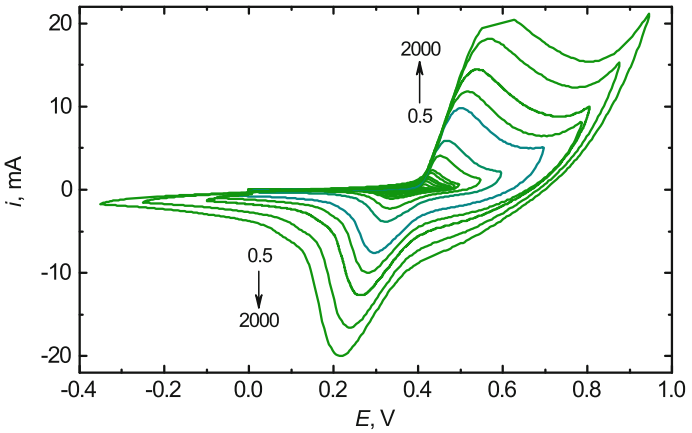

Fig. 4.4 CVA in $1\,\text{mol}\,\text{L}^{-1}$ KOH on electrode with Ni coating at potential scan rate of $0.5\ldots2000\,\text{mV}\,\text{s}^{-1}$

depends on the square root of the potential sweep rate, reflecting the contribution of proton diffusion (reaction Eq. (4.1)) to electrode reactions of nickel hydroxide oxidation and nickel oxyhydroxide reduction. Figure 4.5 shows CVA in the range of small values of potential scan rates (0.5–$40\,\text{mV}\,\text{s}^{-1}$). The surface of nickel is oxidized less actively than the surface of the alloy and multilayer coatings as the oxidation of surface starts at more positive potentials and the slope of the rising ascending branch is smaller. The peak currents i_p at low potential scan rates are proportional to the potential scan rate v. The surface coverage Γ^* of $Ni(OH)_2$/NiOOH redox species of electrode surface can be calculated using the slope of the $i_p - v$ dependencies by Eq. [29]:

$$i_p = (n^2F^2/4RT)vS\Gamma^*, \tag{4.2}$$

where n is number of transferred electron, F is Faraday constant, and S is apparent area of the electrode.

The surface coverage Γ^* of $Ni(OH)_2$/NiOOH redox species of the alloy and multilayer electrodes are 3.66×10^{-6} and $4.8 \times 10^{-6}\,\text{mol}\,\text{cm}^{-2}$ deriving from the average of the anodic and the cathodic results. The Γ^* of electrode with multilayer surface is 1.31 times higher than Γ^* of electrode with coating of alloy, though the real surface area is exceeded by only 1.05 times. The Γ^* value of the NiCu(ML) coating surface is about one order of magnitude higher as compared to the oxidized surface of porous nickel. It is higher as compared to other nickel-containing surfaces [4, 8], and it is at the level of the Γ^* value of the surface of Ni-B coating modified nanoporous Cu ($3.44\times10^{-6}\,\text{mol}\,\text{cm}^{-2}$, [6]).

When ethanol is added to the alkaline electrolyte a wave of ethanol oxidation (Fig. 4.6, curve 1') is observed in the region of nickel hydroxide oxidation potentials (curve 1). In the same potential region, the surface of the copper electrode (curve

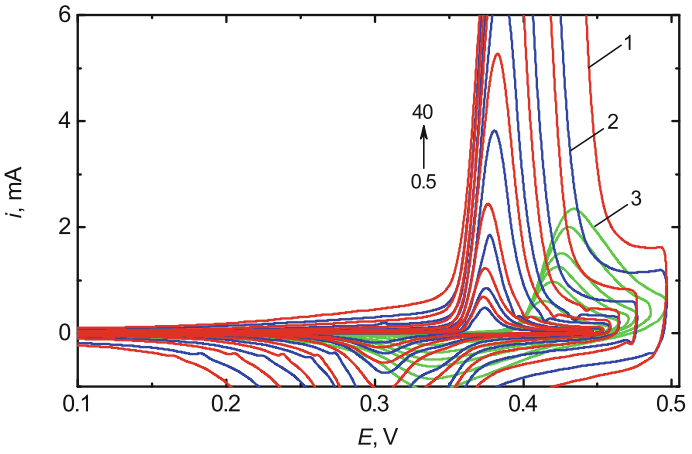

Fig. 4.5 CVA in 1 mol L^{-1} KOH on electrode with NiCu(ML) (1), alloy (2), and Ni (3) coatings, at potential scan rate of 0.0...40 mV s^{-1}

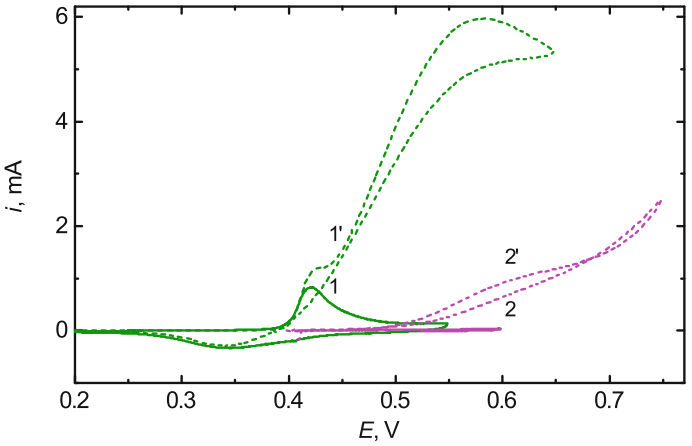

Fig. 4.6 CVA in 1 mol L^{-1} KOH (1, 2) and with the addition of 0.5 mol L^{-1} ethanol (1', 2') on copper (2, 2') and nickel-coated (1, 1') electrodes. Potential scan rate is 10 mV s^{-1}

2) practically does not show catalytic activity (curve 2'), though its geometric area (3.1 cm^2) exceeding the surface area of the studied electrodes by an order of magnitude, and the real surface area (4.8 cm^2) approximately equals the real surface area of the electrodes with Ni-Cu and NiCu(ML) coatings.

A NiCu(ML) coating shows higher catalytic activity as compared to the porous nickel coating (Fig. 4.7). As the potential scan rate increases, ethanol oxidation peak height decreases (Fig. 4.7a–e). Figure 4.7f shows the change in the coefficient k reflecting the relative increase in the ethanol oxidation peak height as compared to the anodic peak height of nickel hydroxide oxidation. A decrease in value of k

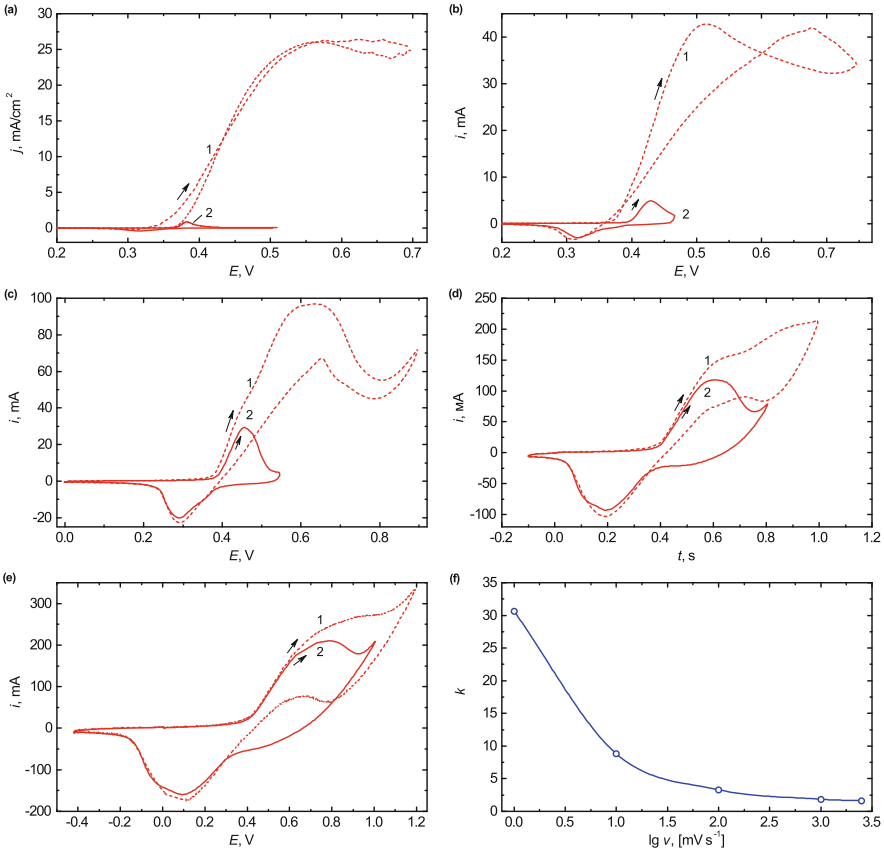

Fig. 4.7 CVA in 1 mol L^{-1} KOH (2) and with the addition of 0.5 mol L^{-1} ethanol (1) on electrode with NiCu(ML) coating at a potential scan rate of 1 mV s^{-1} (**a**), 10 mV s^{-1} (**b**), 100 mV s^{-1} (**c**), 1000 mV s^{-1} (**d**), 2500 mV s^{-1} (**e**); semi-logarithmic dependence (**f**) of the coefficient k (the ratio of the peak current of methanol oxidation to the peak current of nickel hydroxide oxidation) on the potential scan rate

with the increase in potential scan rate indicates slower ethanol oxidation reaction as compared to oxidation reaction of catalytically active surface.

The long-term studies of electrodes in alkali solution (Fig. 4.8, curves 1' and 2') show that the peak height of nickel hydroxide oxidation increases in the first cycles, but in alkaline solution containing alcohol (curves 1 and 2), the peak height of ethanol oxidation in the first cycles decreases. Further cycling in all cases leads to slight increase in peak height. Degradation of the electrodes was not observed. The coefficient k of the relative increase in ethanol oxidation peak height as compared to the peak height of nickel hydroxide oxidation of NiCu(ML) coating ($k = 3.3$) is higher than the value of k for a nickel-copper alloy coating ($k = 2.7$). This indicates

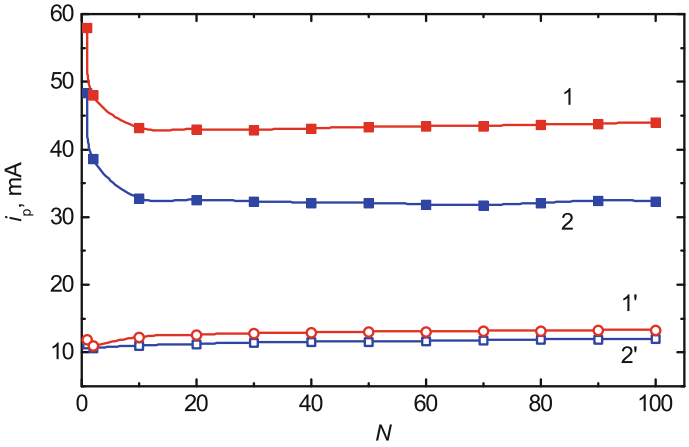

Fig. 4.8 Change in the anode peak current in 1 mol L^{-1} KOH (1', 2') and in 1 mol L^{-1} KOH with the addition of 0.5 mol L^{-1} ethanol (1, 2) when cycling in the potential range of 0.0…+0.7 V at the potential scan rate of 50 mV s^{-1}

a higher catalytic activity of the electrode with a multilayer coating as compared to the electrode with alloy layer.

4.4 Conclusions

A multilayer nickel-copper metal hydroxide electrode coating obtained from a polyligand pyrophosphate-ammonia electrolyte and consisted of alternating layers of nickel-copper alloy and a mixture of metals with hydroxides has higher developed surface, higher surface coverage of redox species, and higher catalytic activity as compared to alloy coating deposited from the same electrolyte.

References

1. Ong BC, Kamarudin SK, Basri S (2017) Direct liquid fuel cells: a review. Int J Hydrog Energy 42:10142–10157. https://doi.org/10.1016/j.ijhydene.2017.01.117
2. Bezghiche-Imloul T, Hammache-Makhloufi H, Aitahmed N (2016) Electrocatalytic oxidation of alcohols on Cu2O/Cu thin film electrodeposited on titanium substrate. Surf Rev Lett 23(5):1650041. https://doi.org/10.1142/S0218625X16500414
3. Barbosa AFB, Oliveira VL, van Drunen J, Tremiliosi-Filho G (2015) Ethanol electro-oxidation reaction using a polycrystalline nickel electrode in alkaline media: temperature influence and reaction mechanism. J Electroanal Chem 746:31–38. https://doi.org/10.1016/j.jelechem.2015.03.024

4. Ehsani A, Mahjani MG, Jafarian M, Naeemy A (2012) Electrosynthesis of polypyrrole composite film and electrocatalytic oxidation of ethanol. Electrochim Acta 71:128–133. https://doi.org/10.1016/j.electacta.2012.03.107
5. Zhang J, Li Q, Zhang J, Fan Y (2016) Advanced anode catalysts for direct alcohol fuel cells. In: Wang Y (ed) Nanomaterials for direct alcohol fuel cell. Pan Stanford Publishing, Singapore, pp 15–76
6. Zhang SJ, Zheng YX, Yuan LS, Zhao LH (2013) Ni-B amorphous alloy nanoparticles modified nanoporous Cu toward ethanol oxidation in alkaline medium. J Power Sources 247:28–436. https://doi.org/10.1016/j.jpowsour.2013.08.129
7. Nikiforova TG, Stepanova AA, Datskevich OA, Maleev VV (2013) Porous nickel deposits formed in the oxidation of alcohols in an alkaline medium. Rus J Appl Chem 86(11):1713–1718. https://doi.org/10.1134/S107042721311013X
8. Hassan HB, Hamid ZA (2011) Electrodeposited Ni-Cr2O3 nanocomposite anodes for ethanol electrooxidation. Int J Hydrog Energy 36(8):5117–5127. https://doi.org/10.1016/j.ijhydene.2011.01.024
9. Li YS, Zhao TS, Liang ZX (2009) Performance of alkaline electrolyte-membrane-based direct ethanol fuel cells. J Power Sources 187(2):387–392. https://doi.org/10.1016/j.jpowsour.2008.10.132
10. Kim JW, Park SM (2005) Electrochemical oxidation of ethanol at nickel hydroxide electrodes in alkaline media studied by electrochemical impedance spectroscopy. J Korean Electrochem Soc 8(3):117–124. https://doi.org/10.5229/JKES.2005.8.3.117
11. Kim JW, Park SM (2003) In situ XANES studies of electrodeposited nickel oxide films with metal additives for the electro-oxidation of ethanol. J Electrochem Soc 150(11):E560–E566. https://doi.org/10.1149/1.1613671
12. Sincheskul A, Pancheva H, Loboichenko V, Avina S, Khrystych O, Pilipenko A (2017) Design of the modified oxide-nickel electrode with improved electrical characteristics. East Eur J Enterp Technol 5(6):23–28
13. Heli H, Jafarian M, Mahjani MG, Goba F (2004) Electro-oxidation of methanol on copper in alkaline solution. Electrochim Acta 49:4999–5006. https://doi.org/10.1016/j.electacta.2004.06.015
14. Yuan LS, Zheng YX, Jia ML, Zhang SJ, Wang XL, Peng C (2015) Nanoporous nickel-copper-phosphorus amorphous alloy film for methanol electro-oxidation in alkaline medium. Electrochim Acta 154:54–62. https://doi.org/10.1016/j.electacta.2014.12.055
15. Sen Gupta S, Mahapatra SS, Datta J (2004) A potential anode material for the direct alcohol fuel cell. J Power Sources 131:169–174. https://doi.org/10.1016/j.jpowsour.2004.01.009
16. Antolinia E, Gonzalez ER (2010) Alkaline direct alcohol fuel cells. J Power Sources 195:3431–3450. https://doi.org/10.1016/j.jpowsour.2009.11.145
17. Danaee I, Jafarian M, Forouzandeh F, Gobal F, Mahjani MG (2008) Electrocatalytic oxidation of methanol on Ni and NiCu alloy modified glassy carbon electrode. Int J Hydrog Energy 33:4367–4376. https://doi.org/10.1016/j.ijhydene.2008.05.075
18. Jafarian M, Moghaddam RB, Mahjani MG, Gobal F (2006) Electro-catalytic oxidation of methanol on a Ni-Cu alloy in alkaline medium. J Appl Electrochem 36(8):913–918. https://doi.org/10.1007/s10800-006-9155-6
19. Jin GP, Ding YF, Zheng PP (2007) Electrodeposition of nickel nanoparticles on functional MWCNT surfaces for ethanol oxidation. J Power Sources 166(1):80–86. https://doi.org/10.1016/j.jpowsour.2006.12.087
20. Zhang S, Zheng Y, Yuan L, Wang X, Zhao L (2014) In situ synthesis of nickel-boron amorphous alloy nanoparticles electrode on nanoporous copper film/brass plate for ethanol electro-oxidation. Int J Hydrog Energy 39(7):3100–3108. https://doi.org/10.1016/j.ijhydene.2013.12.116
21. Maizelis AA, Tul'skii GG, Bairachnyi VB, Trubnikova LV (2017) The effect of ligands on contact exchange in the NdFeB-Cu^{2+}-$P_2O_7^{4-}$-NH_4^+ system. Russ J Electrochem 53(4):417–423. https://doi.org/10.1134/S1023193517040085

22. Fletcher S, Halliday CS, Gates D, Westcott M, Lwin T, Nelson G (1983) The response of some nucleation/growth processes to triangular scans of potential. J Electroanal Chem Interfacial Electrochem 159(2):267–285. https://doi.org/10.1016/S0022--0728(83)80627-5
23. Maizelis AA, Bairachniy BI, Trubnikova LV, Savitsky BA (2012) The effect of architecture of the Cu/(Ni-Cu) multilayer coatings on their microhardness. Funct Mater 19(2):238–244
24. Maizelis AA, Bairachniy BA (2017) Copper nucleation on nickel from pyrophosphate-based polyligand electrolyte. In: International conference on nanotechnology and nanomaterials. Springer, Cham, pp 443–457. https://doi.org/10.1007/978-3-319-92567-7_28
25. Maizelis A, Bairachniy B (2016) Electrochemical formation of multilayer metal and metal oxide coatings in complex electrolytes. In: International conference on nanotechnology and nanomaterials. Springer, Cham, pp 557–572. https://doi.org/10.1007/978-3-319-56422-741
26. Gira MJ, Tkacz KP, Hampton JR (2016) Physical and electrochemical area determination of electrodeposited Ni, Co, and NiCo thin films. Nano Convergence 3(1):6. https://doi.org/10.1186/s40580-016-0063-0
27. Maizelis A, Bairachny B (2017) Voltammetric analysis of phase composition of Zn-Ni alloy thin films electrodeposited from weak alkaline polyligand electrolyte. J Nano-Electron Phys 9(5):1–7. https://doi.org/10.21272/jnep.9(5).05010
28. Maizelis A (2017) Voltammetric analysis of phase composition of Zn-Ni alloy thin films electrodeposited under different electrolyze modes. In: IEEE 7th international conference on nanomaterials: applications and properties 02NTF13. IEEE. https://doi.org/10.1109/NAP.2017.8190373
29. Bard AJ, Faulkner LR (2005) Electrochemical methods, fundamentals and applications. Chemical Industry Press, Beijing, p 409